Supporting Information

Triaxial Braided Piezo Fibers Energy Harvesters for Self-Powered Wearable Technologies

Fatemeh Mokhtari[1], *Javad Foroughi*[1*], *Tian Zheng*[1], *Zhenxiang Cheng*[2], *Geoffrey M. Spinks*[1*]

[1]Intelligent Polymer Research Institute, Wollongong NSW, 2522, Australia
[2]Institute for Superconducting and Electronic Materials, University of Wollongong, Wollongong NSW, 2522, Australia

*Corresponding authors: foroughi@uow.edu.au, gspinks@uow.edu.au

Melt-spinning of PVDF fibers

For controlled cooling of the filaments, an infrared (IR) lamp was used to maintain heat on the filaments as they were extruded from the die. The IR lamp temperature was set at 80 ºC and the mean un-stretched filament diameter was reduced to 400 μm. Further drawing was then applied to the fibers in the solid state at a temperature above T_g but below T_m. The ratio of the β phase to the α phase is known to be very dependent on the temperature of the fiber at the time of drawing and also on the drawing ratio. Here, the fibers were cold-drawn with a draw ratio of 2 (diameter size) at a temperature of 80 °C as they were spun onto a collection drum and the final diameter stretched fiber in this stage was 170-200 μm . During stretching, filament whitening was observed, indicating the onset of a phase transformation in the fiber material.

Movie S1: Movie showing the fabricating piezoelectric PVDF fiber through melt-spinning process.

Poling process

The PVDF chains have a net dipole moment, pointing from the electronegative fluorine to the electropositive hydrogen, producing a net dipole moment nearly perpendicular to the polymer chain. These chains can crystallize in a quasi-hexagonal close-packed β phase structure with dipoles of all chains aligned in a structure with maximum polarization. Poling and switching are accomplished by applying a large electric field perpendicular to the chains to reverse the direction of polarization.

For efficient poling process, the electric field E (E = V/Z, where Z is the PVDF filament thickness and V is the applied voltage) should be close to the dielectric strength which depends on the PVDF filament diameter. The dielectric strength is 45 MV/m to 100 MV/m for a PVDF filament of 170-200 μm diameter which is close to the coercive field for PVDF and its copolymers which range between 50 and 120 MV/m.[1] Care must be taken during this experimental process to avoid flashover or arcing between the electrodes, therefore an insulating rubber tape was placed around the electrode area to serve as an electrical barrier. A small length of one end of the fabricated PVDF braid was modified to expose the core, which served as the inner electrode. The outer sheath was used as the other electrode for the poling process and electrical connection was made at the opposite end of the sample from where the core electrode was connected. The sample was heated to 80 °C for 5 min before the voltage was applied and cooled down to room temperature before the voltage was removed. The applied voltage for the PVDF braid was 25 kV DC.

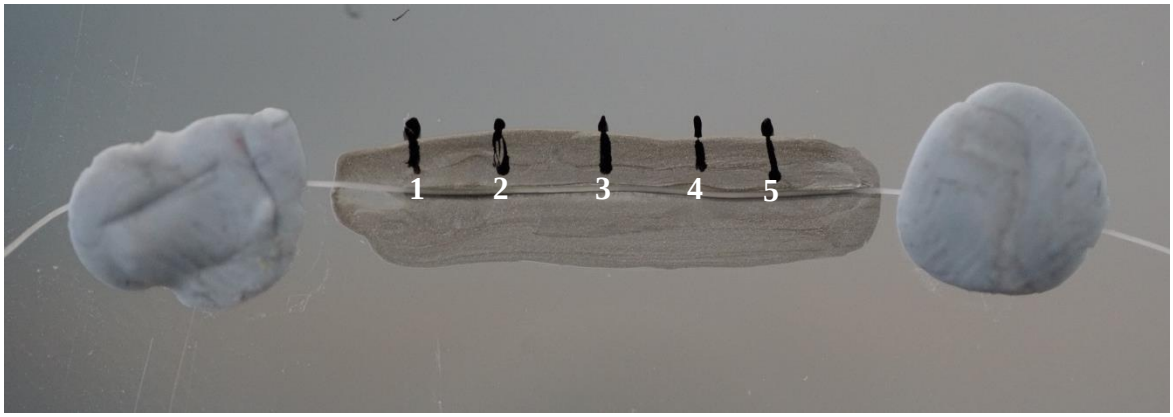

Figure S1. PVDF filament mounted by the silver paste for PFM test

During the PFM test, when the DC bias field is zero (Point A in Fig. S2), the remnant polarization is positive and a detectable amplitude can be obtained. When a positive DC field is applied (Point B in Fig. S2), the positive polarization is enhanced, since the PVDF electrets experience a barrier discharge. Thus, the amplitude is greatly increased and the phase remains the same as that at Point A.

When the voltage decreases, the amplitude will also decrease due to an inverse barrier discharge in the PVDF filament. When the DC field changes to negative (Point C in Fig. S2), the polarization reverses to be negative but its magnitude is considerably smaller than the

value at Point B as a result of the large positive internal bias field induced during corona poling. Therefore, the amplitude at Point C is considerably smaller than that at Point B, leading to the strongly asymmetric amplitude butterfly curve shown in Fig. S2(a). Meanwhile, as the polarization direction at Point C is opposite to that at Point B, the phase difference[2] is 180^{o} ,which is also close to the experimental observations in Figure 7.

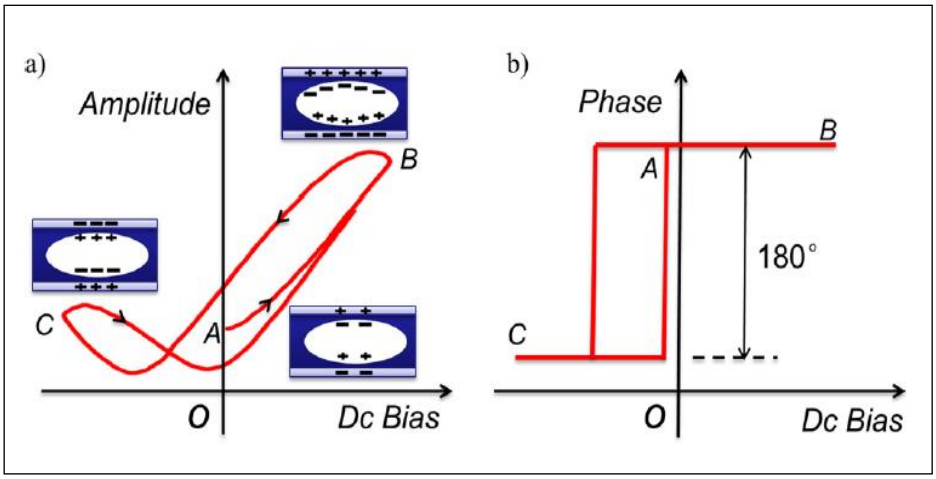

Figure S2. Mechanism of amplitude butterfly curve and phase hysteresis Loop of cellular PP thin film during SS-PFM testing.[2]

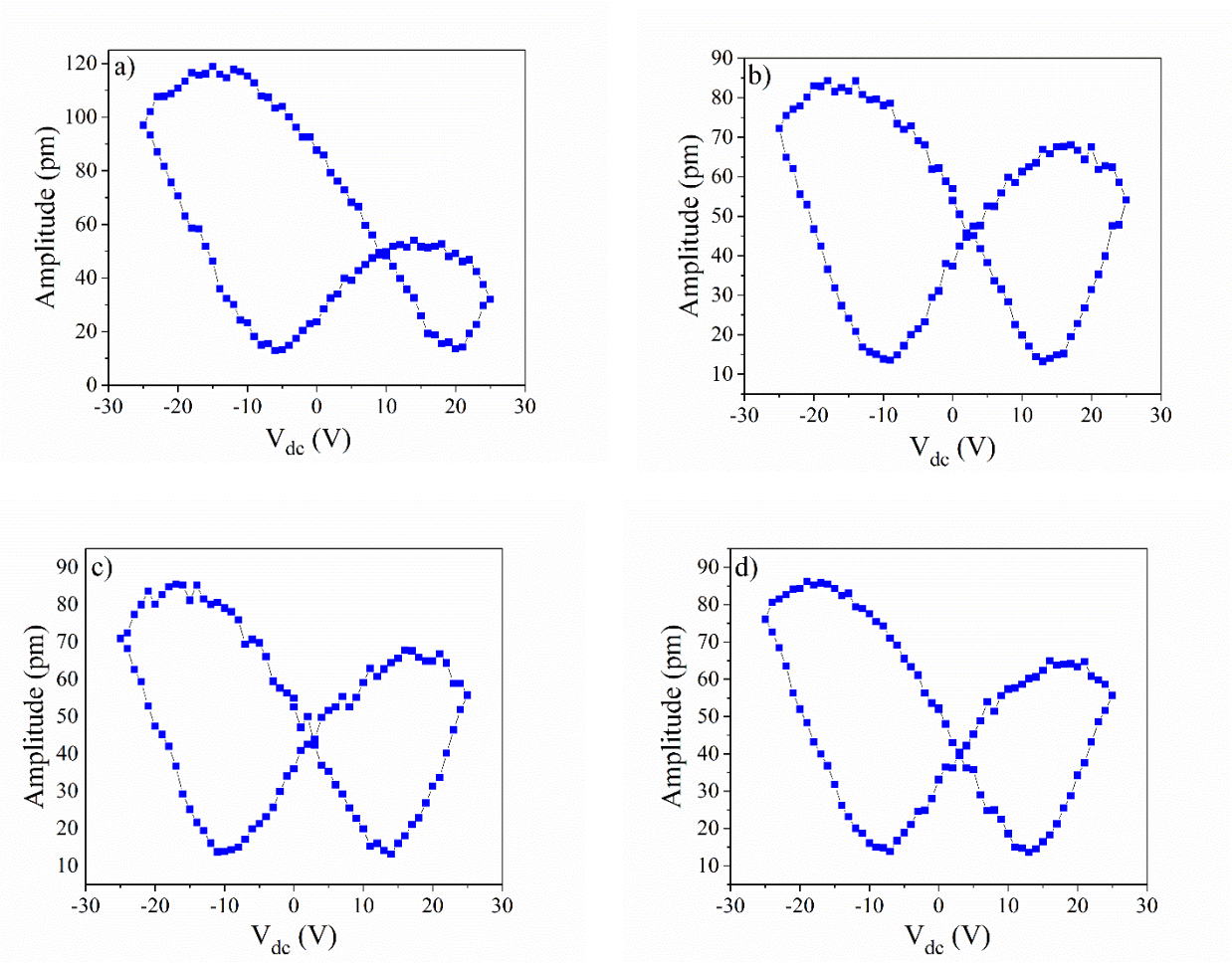

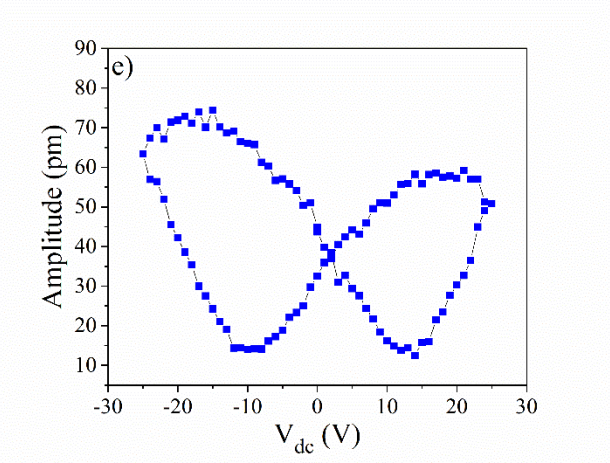

Figure S3. Amplitude butterfly curve test results for the as-prepared poled PVDF fiber with 10 mm length at 5 positions along the length (see Figure S1); from a) to e) respectively.

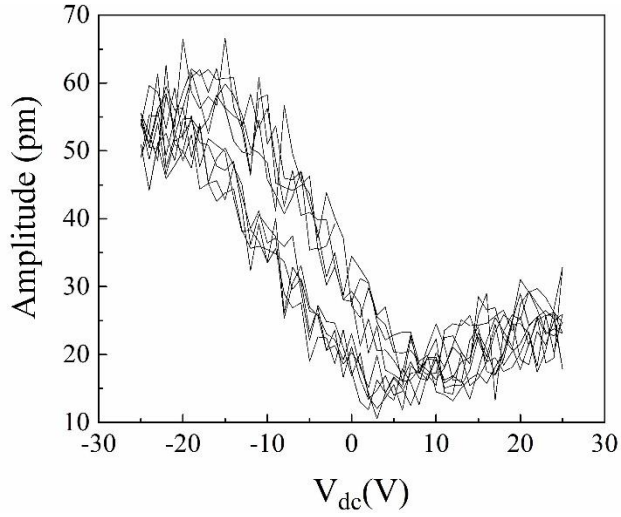

Figure S4. Amplitude butterfly curve test results for the as-prepared poled PVDF fiber with 10 mm length in horizontal direction (cross section).

The local polarization which is done by PFM lithography demonstrates that the dipoles can be switched when subjected to a voltage higher than the excitation field in SS-PFM. However, the switching behavior is already confirmed by SS-PFM in this paper.

Fourier Transform Infrared Spectroscopy (FTIR) Analysis

The FTIR spectra of the melt-spun filaments, stretched and poled PVDF fibers and the starting powder are shown in Figure S5 and Table S1. It can be clearly observed that the starting powder consists primarily of the α-phase, as is evident from the strong characteristic bands at 532, 764, 796, 976, 1215 and 1385 cm^{-1} for the alpha phase.[3] For poled melt-spun fibers, the emergence of peaks at 840 (CH_2 rocking), 1276 (trans band) and 1430 (CH_2

bending) cm^{-1} corresponding to the β phase can be clearly observed, along with a corresponding decrease in the peak at 760 cm^{-1}. The βphase can be well identified from the peak at 1276 cm^{-1}. The peaks at 511 and 840 cm^{-1} corresponds to both β- and γ-phases.[4, 5] Similar results have been observed by various authors where it was shown that both the stretching temperatures (80–100 °C), as well as the drawing ratios, have an effect on the β-phase content. It has been suggested by Lund et al.[6] that an increase in the drawing ratio leads to a higher conversion from the α-phase to the β-phase with a strong correlation between the drawing speeds and the conversion between the phases.[6]

During melt extrusion of the PVDF monofilaments, the filaments were subjected to uniaxial drawing at moderate to high rates, depending upon the take-up speed on the winder. This uniaxial drawing introduced a strong axial flow creating molecular orientation along the drawing direction, leading to an increase in crystallization. This crystallization also changed the morphology of the structure from spherulitic (predominantly α phase and at low drawing ratios) to more fibril like (predominantly β phase and at high drawing ratios) at higher speeds.[1] To determine β phase crystallization in every sample, absorbance peaks related to the α and β phase at wavenumbers 764 and 840 cm^{-1} were evaluated. The level of β phase crystallization was calculated from Equation 1. Here, A_α and A_β were absorbance for the α and β phase, respectively. X_α and X_β are the degree of crystallization for the α and β phases.[7] As can be seen from Table S1, the stretching and poling processes lead to an increase in β phase formation 75% in the treated fibers compared to only 26.7% in the native PVDF powder. However, because of the melting process parameters and the collecting speed used, the β phase formation is lower in the melt-spun fibers in comparison with the PVDF powder.

$$F_\beta = \frac{X_\beta}{X_\alpha + X_\beta} \times 100 = \frac{A_\beta}{A_\beta + 1.26A_\alpha} \times 100 \quad (1)$$

Table S1. Percentage of β phase formation in all PVDF samples

Sample	A_α	A_β	F_β
PVDF powder	0.044	0.0203	26.7%
Meltspun PVDF	0.0088	0.00801	42.12%
Stretched & Poled PVDF	0.00027	0.000976	75%

FTIR is a well-known method for the analysis and quantitative determination of the crystal structure in PVDF. According to the literature, the vibrational bands at 760, 796, 855, and 976 cm^{-1} are characteristic bands of the α phase, whereas the vibrational band at around 840 cm^{-1} denotes the β phase in PVDF.[8] It is very difficult to recognize the specific phase of PVDF on the basis of the IR peaks at 840 and 510 cm^{-1}, because these peaks are dual characteristic peaks corresponding to the β phase as well as to the γ phase. Therefore, the appearance of these bands at 840 and 510 cm^{-1} is a prerequisite to identify the β phase in PVDF, therefore it is never conclusive if the 1279 cm^{-1} vibrational band does not exist in the FT-IR spectra.[3]

As shown in the FTIR spectrum for PVDF powder in Figure S5a, the absorption bands corresponding to the α phase clearly appear in the spectrum and are quite strong. In contrast, the absorption bands which are attributed to the β phase are weak, which indicates that the α phase is dominant in the PVDF powder. Results also showed that the degree of crystallinity in the filaments was determined by the melt draw ratio. Before the cold drawing process (at 80ºC) the crystalline structure of the fibers was predominantly in the α form after which the stretching and poling process lead to an increase in the β phase formation to 75%. (Figure S5b)

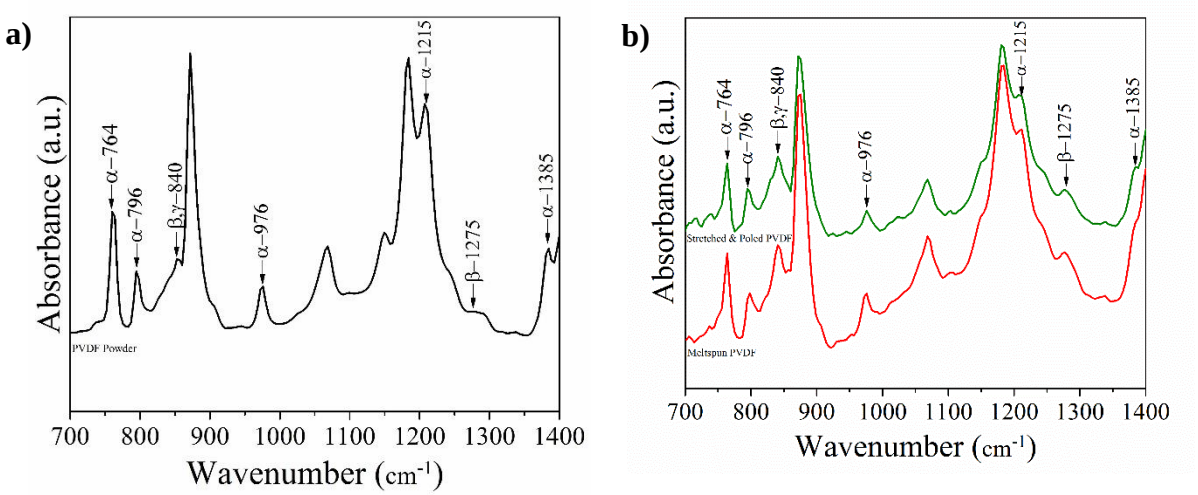

Figure S5: FTIR results for: a) PVDF powder, b) as-prepared meltspun and stretched / poled PVDF filament.

XRD Analysis

To enhance the piezoelectric properties in the PVDF filament, the β-phase crystalline should be present in higher concentrations since it displays the most effective piezoelectricity. Hence, X-ray diffraction (XRD) of the samples (meltspun filament, stretched and poled

PVDF and the starting powder) was performed to evaluate the formation of this phase. X-ray diffraction is one of the most important characterization tools used in solid state chemistry and materials science. XRD patterns provide information on the long-range order and the crystal structure of random networks. Figure S5 illustrates the XRD diffractograms of a typical β crystal phase peak at around $2\theta = 20°$ which is assigned to the total diffraction in (110) and (200) planes. The peak at 18.30° corresponds to the reflection of the (020) plane of the α-phase.[1] The ratio intensity of β to α phase is increased from 1.21 to 1.58 for the meltspun PVDF compared to stretched and poled PVDF filaments. Hence, this may suggest that most of the crystal phase in stretched and poled PVDF filament has been changed to β-phase by the cold drawing (at a temperature of 80ºC) and poling process, whereby the β-phase crystal structure becomes dominant with some transitions or mixtures of α and β phases. The ratio intensity for PVDF powder (1.63) is higher than meltspun filament (1.21) because the α phase peak intensity for the meltspun PVDF filament is higher than in the PVDF powder. As previously explained, during melt-spinning of the filaments the collecting speed was low which leads to higher α phase formation in the melt-spun fiber when compared to the powder. The level of β phase formation is related to the take-up speed of the collector and axial drawing of filaments and so this phase is more predominant in stretched and poled PVDF filaments.

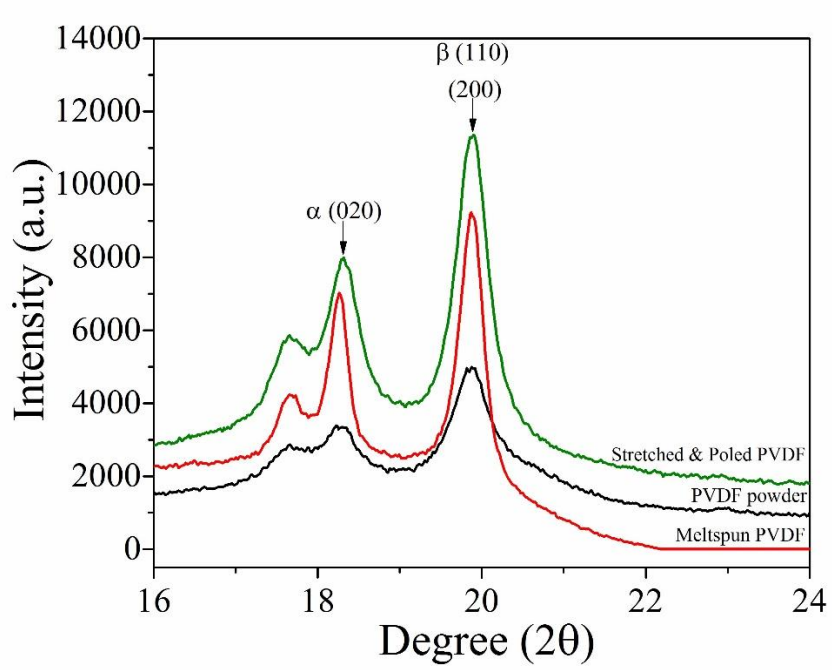

Figure S6: X-ray diffraction patterns results for powder, as-prepared meltspun, stretched and poled PVDF filament.

Thermal Analysis Using DSC

Further investigation of the PVDF powder and filaments was carried out by measuring the melting temperature and melting enthalpy using DSC (Figure S6). Based on the DSC thermograms, the melting temperature (T_m) of stretched and poled PVDF filaments (170.76 °C) was lower than the meltspun PVDF filaments (172.73 °C). This indicates that more crystals had been formed during the cold drawing process. The crystalline structure of β-phase PVDF has a lower melting temperature than α-phase PVDF.[9] It can also be seen from Figure 6 that the melting enthalpy of stretched and poled PVDF filaments ($\Delta H_m = 74.46$ J g^{-1}) is more than the meltspun PVDF filaments (70.60 J g^{-1}). These results confirmed that the formation of the β phase crystalline structure in the stretched and poled PVDF filaments is higher than in the meltspun filaments (around 67.5% for meltspun PVDF filaments and 71.2% for stretched and poled PVDF filaments). Gheibi et al.[10] have done the same analysis in a comparison of β-phase formation in electrospun PVDF nanofiber mats and granules. The melting enthalpy of PVDF nanofibers ($\Delta H_m = 68.22$ J g^{-1}) is much more than that of the granules (41.70 J g^{-1}). As a result, there is an increase in crystallinity for electrospun nanofiber mats, which confirmed the formation of a new crystalline structure (β phase) in electrospun nanofiber mats.[10] The degree of crystallinity, ΔH_c was measured as the ratio between ΔH_m and ΔH_{100} , where ΔH_{100} is the melting enthalpy of totally crystalline PVDF material (ΔH_{100}=104.5 J $g^{-1}$for α phase and ΔH_{100} =103.4 J g^{-1} for β-phase by using the equation 2 as below:[11]

$$\Delta Hc = \frac{\Delta Hm}{\Delta H100} \times 100 \quad (2)$$

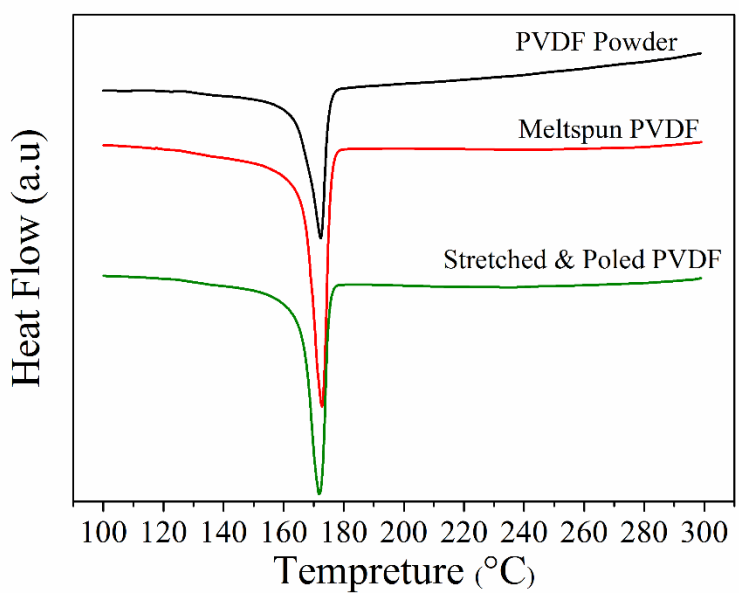

Figure S7: DSC patterns for powder, Melt-spun, Stretched and Poled PVDF filaments

Mechanical Properties

In fiber production, melt spinning is generally followed by cold drawing (drawing at a temperature below the crystal melting point) of the fiber, as undrawn fibers exhibit poor mechanical properties, such as low stiffness, high strain to break, and high irreversible extensibility. Drawing is an irreversible elongation of an as-spun material in the solid state.

Both cold-drawn and non-stretched PVDF filaments were mechanically tested to determine the effect of longitudinal stretching on the polymer filament (Figure 4c). Tenacity test results show that tensile strength of stretched PVDF filament is higher than Non-stretched PVDF filament. Hadimani et al.[12] did mechanical test for poled and unpoled PVDF filament the results showed that higher force needed to break the poled PVDF fibers which proved that poling process increased the strength of PVDF fibers. Gomes et al.[13] have studied the effect of stretching ratio and temperature on α to β phase transformation in PVDF. They observe that variations in the phase content are accompanied by changes in the degree of crystallinity and the microstructure of the material, and these changes have a significant impact on the macroscopic piezoelectric and ferroelectric response of the material.

Table S2. Measurement results taken from the Shimadzu tensile tester

	Stress (MPa)	Strain (%)	Young's modulus (MPa)
Non-Stretched filament	37	178	354
Stretched filament	110	58	843

The sensitivity of the as-prepared triaxial piezoelectric textiles was evaluated using output voltage divided by the applied force [14] (see Figure S7 and Movie S2). The results indicated that the triaxial piezo energy generator exhibited an almost 4-fold increase in value (1.6 V/N) compared to those previously reported.[15]

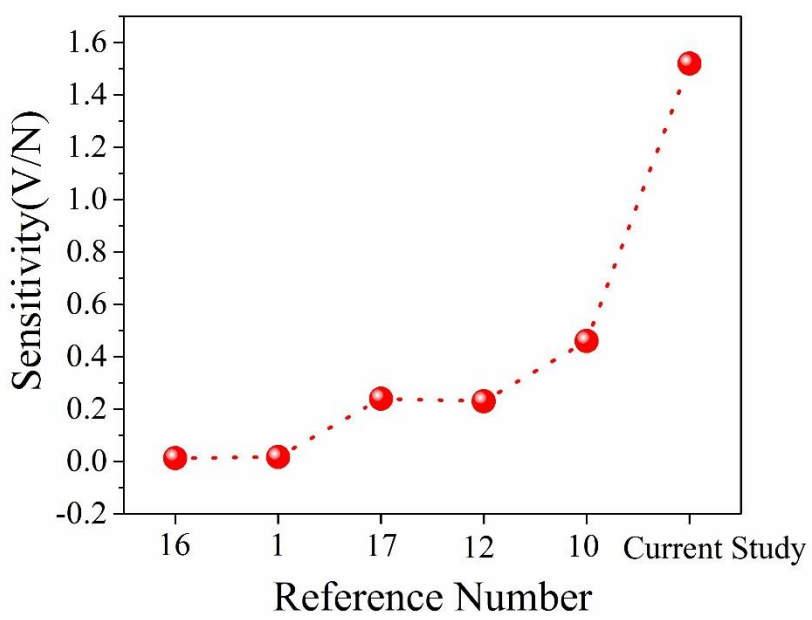

Figure S8. Diagram to compare sensitivity results from this study to previous published work for pure PVDF [1, 10, 12, 16, 17].

Movie S2: The movie showing a piezoelectric response (Sensitivity) using a triaxial braided textile as mechanical energy harvester. (Finger Responses)

Movie S3: The movie showing the developed triaxial braided textile energy generator by generating voltage can charge a commercial battery or capacitor from tensile and bending deformations.(Bending elbow)

References

[1] N. Soin, T.H. Shah, S.C. Anand, J. Geng, W. Pornwannachai, P. Mandal, D. Reid, S. Sharma, R.L. Hadimani, D.V. Bayramol, Energy Environ. Sci. **2014**, *7*, 1670.

[2] H. Miao, Y. Sun, X. Zhou, Y. Li, F. Li, J. Appl. Phys. **2014**, *116*, 066820.

[3] D. Mandal, K. Henkel, D. Schmeisser, The Journal of Physical Chemistry B. **2011**, *115*, 10567-10569.

[4] B.S. Ince-Gunduz, R. Alpern, D. Amare, J. Crawford, B. Dolan, S. Jones, R. Kobylarz, M. Reveley, P. Cebe, Polymer. **2010**, *51*, 1485-1493.
[5] S. Ramasundaram, S. Yoon, K.J. Kim, C. Park, Journal of Polymer Science Part B: Polymer Physics. **2008**, *46*, 2173-2187.
[6] A. Lund, B. Hagström, J. Appl. Polym. Sci. **2011**, *120*, 1080.
[7] F. Mokhtari, M. Shamshirsaz, M. Latifi, S. Asadi, J. Text. Inst. **2017**, *108*, 906.
[8] F. Mokhtari, M. Latifi, M. Shamshirsaz, J. Text. Inst. **2016**, *107*, 1037.
[9] F. Mokhtari, M. Shamshirsaz, M. Latifi, Polym. Eng. Sci. **2016**, *56*, 61.
[10] A. Gheibi, M. Latifi, A.A. Merati, R. Bagherzadeh, J. Polym. Res. **2014**, *21*, 1.
[11] C.M. Costa, L.C. Rodrigues, V. Sencadas, M.M. Silva, J.G. Rocha, S. Lanceros-Méndez, J. Membr. Sci. **2012**, *407–408*, 193.
[12] R.L. Hadimani, Adv. Mater. Res. **2012**, *410*,
[13] J. Gomes, J.S. Nunes, V. Sencadas, S. Lanceros-Mendez, Smart Mater. Struct. **2010**, *19*, 065010.
[14] I. Katsouras, K. Asadi, M. Li, T.B. van Driel, K.S. Kjær, D. Zhao, T. Lenz, Y. Gu, P.W.M. Blom, D. Damjanovic, M.M. Nielsen, D.M. de Leeuw, Nat. Mater. **2015**, *15*, 78.
[15] J.C. Kyu, P. Kwi-Il, R. Jungho, H. Geon-Tae, L.K. Jae, Adv. Funct. Mater. **2014**, *24*, 2620.
[16] Y.-C. Wang, Y.-W. Chen, Exp. Therm. Fluid Sci. **2007**, *32*, 403.
[17] R.L. Hadimani, D.V. Bayramol, N. Sion, T. Shah, Q. Limin, S. Shaoxin, E. Siores, Smart Mater. Struct. **2013**, *22*, 075017.